Substantial gain enhancement for optical parametric amplification and oscillation in two-dimensional $\chi^{(2)}$ nonlinear photonic crystals

Hsi-Chun Liu[1,2], and A. H. Kung[1,3]
[1]*Institute of Atomic and Molecular Sciences, Academia Sinica, Taipei 10617, Taiwan*
[2]*Department of Electrical Engineering, California Institute of Technology, Pasadena, CA*
[3]*Department of Photonics, National Chiao Tung University, Hsinchu 30010, Taiwan*
Corresponding author: hliu@caltech.edu

Abstract: We have analyzed optical parametric interaction in a 2D NPC. While in general the nonlinear coefficient is small compared to a 1D NPC, we show that at numerous orientations a multitude of reciprocal vectors contribute additively to enhance the gain in optical parametric amplification and oscillation in a 2D patterned crystal. In particular, we have derived the effective nonlinear coefficients for common-signal amplification and common-idler amplification for a tetragonal inverted domain pattern. We show that in the specific case of signal amplification with QPM by both $\boldsymbol{G}_{10}$ and $\boldsymbol{G}_{11}$, symmetry of the crystal results in coupled interaction with the corresponding signal amplification by $\boldsymbol{G}_{10}$ and $\boldsymbol{G}_{1,-1}$. As a consequence, this coupled utilization of all three reciprocal vectors leads to a substantial increase in parametric gain. Using PPLN we demonstrate numerically that a gain that comes close to that of a 1D QPM crystal could be realized in a 2D NPC with an inverted tetragonal domain pattern. This special mechanism produces two pairs of identical signal and idler beams propagating in mirror-imaged forward directions. In conjunction with this gain enhancement and multiple beams output we predict that there is a large pulling effect on the output wavelength due to dynamic signal build-up in the intrinsic noncollinear geometry of a 2D NPC OPO.

OCIS codes: (190.4970) Parametric oscillators and amplifiers; (160.5298) Photonic crystals.

References and links

1. V. Berger, "Nonlinear photonic crystals", Phys. Rev. Lett. **81**, No. 19, 4136-4139 (1998).
2. N. G. R. Broderick, G.W. Ross, H. L. Offerhaus, D. J. Richardson, and D. C. Hanna, "Hexagonally poled lithium niobate: a two-dimensional nonlinear photonic crystal", Phys. Rev. Lett. **84**, 4345-4348 (2000).
3. L.-H. Peng, C.-C. Hsu, Jimmy Ng, and A. H. Kung, "Wavelength tunability of second-harmonic generation from two-dimensional $\chi^{(2)}$ nonlinear photonic crystals with a tetragonal lattice structure", Appl. Phys. Lett. **84**, 3250-3252 (2004).
4. M. Seiter and M. W. Sigrist, "On-line multicomponent trace-gas analysis with a broadly tunable pulsed difference-frequency laser spectrometer," Appl. Opt. **38**, 4691-4698 (1999).
5. M. H. Chou, I. Brener, G. Lenz, R. Scotti, E. E. Chaban, J. Shmulovich, D. Philen, S. Kosinski, K. R. Parameswaran, and M. M. Fejer, "Efficient wide-band and tunable midspan spectral inverter using cascaded nonlinearities in $LiNbO_3$ waveguides," IEEE Photonics Technology Lett. **12**, 82-84 (2000).
6. L. E. Myers, G. D. Miller, R. C. Eckardt, M. M. Fejer, and R. L. Byer, "Quasi-phase-matched 1.064 micron-pumped optical parametric oscillator in bulk periodically poled $LiNbO_3$", Opt. Lett. **20**, 52-54 (1995).
7. A. Arie, N. Habshoosh, and A. Bahabad, "Quasi phase matching in 2D nonlinear photonic crystals", Opt. Quantum Electron. **39**, 361 (2007).
8. D. H. Jundt, "Temperature-dependent Sellmeier equation for the index of refraction, n_e, in congruent lithium niobate", Opt. Lett. **22**, 1553 (1997).
9. R. W. Boyd, *Nonlinear Optics*, 2nd Ed. Chap. 2 (Academic Press, 2003).

#94772 - $15.00 USD Received 7 Apr 2008; revised 2 Jun 2008; accepted 12 Jun 2008; published 17 Jun 2008

10. L.-H. Peng, C.-C. Hsu, and Y.-C. Shih, "Second-harmonic green generation from two-dimensional $\chi^{(2)}$ nonlinear photonic crystal with orthorhombic lattice structure", Appl. Phys. Lett. **83**, 3447 (2003).
11. A. E. Siegman, *Lasers*, pg 1169, Chapter 29 (University Science Books, 1986).

1. Introduction

In a two-dimensional $\chi^{(2)}$ nonlinear photonic crystal (2D NPC), the sign of $\chi^{(2)}$ is reversed periodically in two directions [1]. This produces a nearly infinite number of reciprocal vectors in the 2D reciprocal lattice. Each reciprocal vector corresponds to one or more phase-matching solution. The 2D structure thus provides a much greater flexibility in the quasi-phase-matching (QPM) of wavelength conversion processes, permitting simultaneous efficient multi-wavelength second harmonic and sum frequency mixing to occur [2,3]. Similarly the 2D NPC makes parametric generation and amplification interesting. The multitude of off-angle reciprocal vectors makes possible either multi-wavelength parametric generation and amplification or the emission of the same generated wavelength in more than one direction. These possibilities may find potentially interesting applications in, for example, simultaneous multiple-trace-gas detection [4] where several wavelengths are required at the same time or in multichannel information processing where efficient cascaded conversion of several wavelengths are necessary [5]. However, parametric generation and amplification in a 2D NPC has not been reported even though 1D NPC QPM optical parametric oscillators (OPOs) were demonstrated from the early days of periodic poling for QPM [6]. This is perhaps because the effective $\chi^{(2)}$ in a 2D NPC is a lot smaller than in the 1D case due to its structure factor [1,7] so that generally the parametric gain would be too small. In view of the potential application of multi-wavelength and multi-directional emissions from 2D NPC parametric generators it is our objective to explore 2D NPC for situations where the parametric gain can be substantially enhanced to turn 2D NPCs into a competitive parametric medium.

We have analyzed optical parametric generation and oscillation in a 2D NPC. In this paper we show that in several circumstances more than one reciprocal vector can act together to provide a higher QPM optical gain. Moreover, in certain geometries the gain can approach that in the 1D case without requiring merging of the structure into a 1D structure. Furthermore a pair of signal (and the idler) beams of identical wavelength can be generated simultaneously and emitted symmetrically on opposite transverse sides of the pump beam. These are unique properties of a 2D NPC parametric device that may find interesting applications in remote sensing or information processing. Here we describe both the theoretical derivation and numerical simulation of these circumstances to guide the design of such a 2D NPC parametric generator or parametric oscillator. The analysis is for a tetragonal inverted domain structure and for the reciprocal vectors $\boldsymbol{G}_{mn}$, m,n =0, ±1 which results in the highest effective parametric gain. However the analysis should be readily generalized to apply to any of the five Bravais structures of the 2D NPC and their complete set of reciprocal vectors.

2. Parametric interaction in 2D NPC

A 2D NPC with a tetragonal inverted domain structure can be represented by a reciprocal lattice shown in Fig. 1. In this lattice structure, the reciprocal vectors $\boldsymbol{G}_{mn}$ are

#94772 - $15.00 USD Received 7 Apr 2008; revised 2 Jun 2008; accepted 12 Jun 2008; published 17 Jun 2008

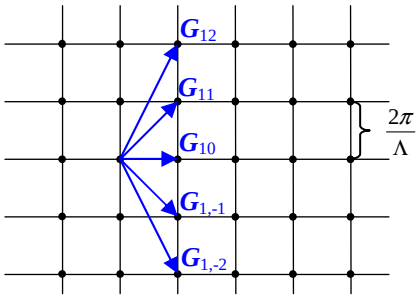

Fig. 1. Reciprocal lattice of a tetragonal structure

$$\boldsymbol{G_{mn}} = m\frac{2\pi}{\Lambda_x}\hat{x} + n\frac{2\pi}{\Lambda_y}\hat{y}\,, \tag{1}$$

where Λ_x and Λ_y are the periodicities along the x and y axes; m and n are integers. For QPM parametric amplification, momentum conservation of the pump, signal, and idler waves gives

$$\boldsymbol{k_p} = \boldsymbol{k_s} + \boldsymbol{k_i} + \boldsymbol{G_{mn}}, \tag{2}$$

where $\boldsymbol{k_p}$, $\boldsymbol{k_s}$, and $\boldsymbol{k_i}$ are the wave vectors of the pump, signal, and idler waves, respectively. Suppose the pump beam propagates parallel to one of the unit vectors in the structure, then the angles of $\boldsymbol{k_p}$ and $\boldsymbol{k_s}$ relative to the unit vector are 0 and θ_s respectively. For a given $\boldsymbol{G}$, Eq. (2) can be written in scalar form as

$$\cos(\theta_s - \theta) = \frac{k^2 + k_s^{\,2} - k_i^{\,2}}{2kk_s} \tag{3}$$

and

$$\cos(\theta_i - \theta) = \frac{k^2 + k_i^{\,2} - k_s^{\,2}}{2kk_i}\,, \tag{4}$$

where $\boldsymbol{k} = \boldsymbol{k_p} - \boldsymbol{G}$, θ and θ_t are the angles of $\boldsymbol{k}$ and $\boldsymbol{k_i}$ respectively. A wavelength vs. θ_s or θ_t curve for $\boldsymbol{G}$ can be constructed from Eq. (3) and (4). Since every reciprocal vector $\boldsymbol{G_{mn}}$ contributes to a tuning curve there is an infinite set of curves for a single 2D NPC parametric generator. In this paper, we focus on the vectors $\boldsymbol{G_{10}}$, $\boldsymbol{G_{11}}$, and $\boldsymbol{G_{1,-1}}$ that have the highest strength and therefore show the most prominent effects. The curves associated with these three vectors are shown in Fig. 2. There are three sets of curves, each set representing a G vector indicated at the degenerate point of the set. These curves are calculated with the Sellmeier equations from reference 8 to serve as an example case and uses 1064 nm as the pump beam with $\Lambda_x = \Lambda_y = 29.5$ μm, and the crystal temperature is 157°C. The curves has a mirror symmetry at $\theta_s = 0$ or $\theta_i = 0$ due to the symmetry of the tetragonal structure. Two features unique to 2D NPC can be discerned from these curves. The first is that for every θ_s or θ_i there can be more than one wavelength that satisfies the QPM condition, meaning multiple wavelengths can have gain in every direction. The second is that there are several locations, some of which are designated by letters C through F in Fig. 2, where the signal curves or the idler curves intersect. At these locations, two reciprocal vectors contribute together to the nonlinear interaction of generating the signal or the idler wavelength. The parametric gain there can therefore be expected to be enhanced as we shall see in the next section.

#94772 - $15.00 USD Received 7 Apr 2008; revised 2 Jun 2008; accepted 12 Jun 2008; published 17 Jun 2008

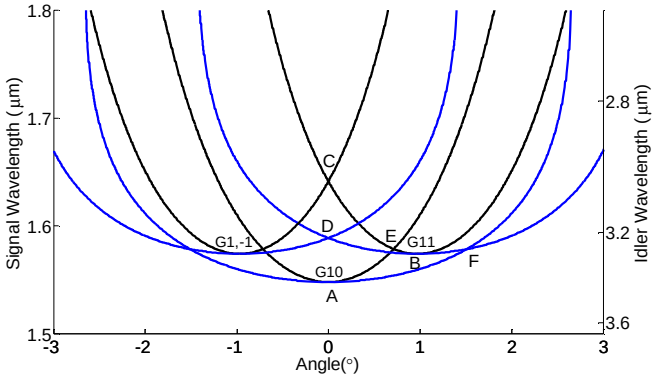

Fig. 2. the wavelength- $\theta_s(\theta_i)$ diagram of $\boldsymbol{G}_{10}$, $\boldsymbol{G}_{11}$, and $\boldsymbol{G}_{1,-1}$. Black lines are the signal, while blue lines are the idler.

3. Theoretical derivation of the parametric gain

Assume that all of the electric fields are along the z-axis, and the waves are propagating along the x-axis, and suppose the pump, signal, and idler are plane waves and that there is no walk-off problem, i.e., the beam radiuses are large compared to the length of interaction, and further assuming slowly varying amplitudes and paraxial propagation, then the parametric interaction can be described by the following coupled equations [9]:

$$\begin{aligned}
\frac{dE_p(x)}{dx} &= -i\frac{2\mu_0 w_p^{\,2}}{k_p} d_{33}(\boldsymbol{r}) E_s(x) E_i(x) \exp[i\Delta\boldsymbol{k}\cdot\boldsymbol{r}] \\
\frac{dE_s(x)}{dx} &= -i\frac{2\mu_0 w_s^{\,2}}{k_s} d_{33}(\boldsymbol{r}) E_p(x) E_i^{*}(x) \exp[-i\Delta\boldsymbol{k}\cdot\boldsymbol{r}], \\
\frac{dE_i(x)}{dx} &= -i\frac{2\mu_0 w_i^{\,2}}{k_i} d_{33}(\boldsymbol{r}) E_p(x) E_s^{*}(x) \exp[-i\Delta\boldsymbol{k}\cdot\boldsymbol{r}]
\end{aligned} \tag{5}$$

where $E_p(x)$, $E_s(x)$, and $E_i(x)$ are the electric field amplitudes in $\boldsymbol{E}(\boldsymbol{r}) = \hat{z}E(x)\exp[i(wt-\boldsymbol{k}\cdot\boldsymbol{r})]$, and $\Delta\boldsymbol{k} = \boldsymbol{k_p} - \boldsymbol{k_s} - \boldsymbol{k_i}$ is the momentum mismatch. In a 2D NPC, the nonlinear coefficient $d_{33}(\boldsymbol{r})$ can be expressed in the form of a Fourier series [1]:

$$d_{33}(\boldsymbol{r}) = d_{33}\sum_{m=-\infty}^{\infty}\sum_{n=-\infty}^{\infty} a_{mn}\exp[i\boldsymbol{G_{mn}}\cdot\boldsymbol{r}], \tag{6}$$

where $\boldsymbol{G_{mn}}$ are the reciprocal vectors. The phase term $\exp[-i\Delta\boldsymbol{k}\cdot\boldsymbol{r}]$ in Eq. (5) is cancelled by the phase term of $d_{33}(\boldsymbol{r})$ if one of the reciprocal vectors $\boldsymbol{G_{mn}}$ is equal to $\Delta\boldsymbol{k}$. In the absence of pump depletion, $E_p(x)$ is a constant. Eq. (5) leads to

$$\frac{d^2E_s(x)}{dx^2} = \frac{4\mu_0^{\,2}w_s^{\,2}w_i^{\,2}d_{33}^{\,2}\left|E_p\right|^2}{k_s k_i}\cdot\left|a_{mn}\right|^2 E_s(x). \tag{7}$$

Letting $E_i(0) = 0$ gives the solution:

$$E_s(x) = E_s(0)\cosh(gx), \tag{8}$$

#94772 - $15.00 USD Received 7 Apr 2008; revised 2 Jun 2008; accepted 12 Jun 2008; published 17 Jun 2008

where
$$g = \frac{2\mu_0 w_s w_i d_{33} |E_p|}{\sqrt{k_s k_i}} \cdot |a_{mn}| \tag{9}$$

This is equivalent to the standard parametric gain expression for birefringent phase-matched interaction with an effective nonlinear coefficient $d_{eff} = |a_{mn}| d_{33}$.

Common-signal amplification: In the case when two reciprocal vectors $\boldsymbol{G_1}$ and $\boldsymbol{G_2}$ with strength a_1 and a_2 couple the pump beam to the same signal field E_s such as point C in Fig. 2 so that the signal wavelength is the same but the idlers E_{i1} and E_{i2} have different propagating directions, the coupled equations become

$$\begin{aligned}
\frac{dE_s(x)}{dx} &= -i\frac{2\mu_0 w_s^2 d_{33} E_p}{k_s}(a_1 E_{i1}^*(x) + a_2 E_{i2}^*(x)) \\
\frac{dE_{i1}(x)}{dx} &= -i\frac{2\mu_0 w_i^2 d_{33} E_p}{k_i} a_1 E_s^*(x) \\
\frac{dE_{i2}(x)}{dx} &= -i\frac{2\mu_0 w_i^2 d_{33} E_p}{k_i} a_2 E_s^*(x)
\end{aligned} \quad . \tag{10}$$

With $E_{i1}(0) = E_{i2}(0) = 0$, the amplification to E_s is the solution $E_s(x) = E_s(0)\cosh(gx)$, where

$$g = \frac{2\mu_0 w_s w_i d_{33} |E_p|}{\sqrt{k_s k_i}} \cdot \sqrt{|a_1|^2 + |a_2|^2} \, . \tag{11}$$

Hence effective nonlinear coefficient is $d_{eff} = \sqrt{|a_1|^2 + |a_2|^2}\, d_{33}$ which is larger than that given in Eq. (9). The result shows that the increase is due to a simple addition of contribution from two paths of interaction.

Common-idler gain: Similarly when two reciprocal vectors $\boldsymbol{G_1}$ and $\boldsymbol{G_2}$ with strength a_1 and a_2 coupling the pump beam to a common idler E_i but two signals E_{s1} and E_{s2}, which have the same wavelength but different propagating directions (point D in Fig. 2), the coupled equations then are

$$\begin{aligned}
\frac{dE_{s1}(x)}{dx} &= -i\frac{2\mu_0 w_s^2 d_{33} E_p}{k_s} a_1 E_i^*(x) \\
\frac{dE_{s2}(x)}{dx} &= -i\frac{2\mu_0 w_s^2 d_{33} E_p}{k_s} a_2 E_i^*(x) \\
\frac{dE_i(x)}{dx} &= -i\frac{2\mu_0 w_i^2 d_{33} E_p}{k_i}(a_1 E_{s1}^*(x) + a_2 E_{s2}^*(x))
\end{aligned} \quad . \tag{12}$$

The solution to Eq. (12) assuming $E_{s1}(0) = E_{s2}(0) = 0$ is $E_i(x) = E_i(0)\cosh(gx)$ where g is defined in Eq. (11). For amplification of E_{s1} with a common-idler gain, we have $E_{s2}(0) = E_i(0) = 0$ and the solution

$$E_{s1}(x) = E_{s1}(0)\left[\frac{|a_2|^2}{|a_1|^2 + |a_2|^2} + \frac{|a_1|^2}{|a_1|^2 + |a_2|^2}\cosh(gx)\right], \tag{13}$$

#94772 - $15.00 USD Received 7 Apr 2008; revised 2 Jun 2008; accepted 12 Jun 2008; published 17 Jun 2008

where $g = \frac{2\mu_0 w_s w_i d_{33} |E_p|}{\sqrt{k_s k_i}} \cdot \sqrt{|a_1|^2 + |a_2|^2}$ as in Eq. (11). Comparing this to the case of a common signal, the gain coefficient is identical to the common signal case but the signal growth is reduced by a constant factor of $\frac{|a_1|^2}{|a_1|^2 + |a_2|^2}$.

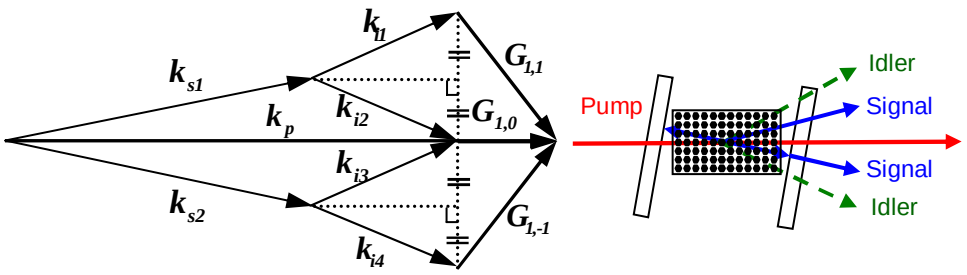

Fig. 3. (Left) Phase-matching condition in point E. (Right) 2D OPG diagram in point E.

In Fig. 2, point C ($\theta_s = 0°$, $\theta_{i1} = 2.8°$, and $\theta_{i2} = -2.8°$) has a common-signal amplification using $\boldsymbol{G_{11}}$ and $\boldsymbol{G_{1,-1}}$. Point D ($\theta_i = 0°$, $\theta_{i1} = 1.4°$, and $\theta_{i2} = -1.4°$) has a common-idler amplification. Point E presents a special situation that is particularly more interesting. At this location the vectors $\boldsymbol{G_{10}}$ and $\boldsymbol{G_{11}}$, and $\boldsymbol{G_{1,-1}}$ are all involved in the amplification process. The phase-matching diagram is shown in the left of Fig. 3 with the output directions of the signal and the idler beams of an OPO shown on the right side of the figure. First, there is the common-signal amplification with $\boldsymbol{G_{10}}$ and $\boldsymbol{G_{11}}$, generating $\boldsymbol{k_{s1}}$, $\boldsymbol{k_{i1}}$, and $\boldsymbol{k_{i2}}$. Because of mirror symmetry, $\boldsymbol{k_{i1}}$ and $\boldsymbol{k_{i2}}$ are exactly the same as $\boldsymbol{k_{i3}}$ and $\boldsymbol{k_{i4}}$ respectively. Consequently, these two idlers generate $\boldsymbol{k_{s2}}$ using $\boldsymbol{G_{10}}$ and $\boldsymbol{G_{1,-1}}$. The two signals and two idlers thus interact *coherently* with each other using QPM from the three reciprocal vectors. The coupled equations are

$$\begin{aligned}
\frac{dE_{s1}(x)}{dx} &= -i\frac{2\mu_0 w_s^2 d_{33} E_p}{k_s}\left(a_{11}E_{i1}^*(x) + a_{10}E_{i2}^*(x)\right)\\
\frac{dE_{s2}(x)}{dx} &= -i\frac{2\mu_0 w_s^2 d_{33} E_p}{k_s}\left(a_{10}E_{i1}^*(x) + a_{1,-1}E_{i2}^*(x)\right)\\
\frac{dE_{i1}(x)}{dx} &= -i\frac{2\mu_0 w_i^2 d_{33} E_p}{k_i}\left(a_{11}E_{s1}^*(x) + a_{10}E_{s2}^*(x)\right)\\
\frac{dE_{i2}(x)}{dx} &= -i\frac{2\mu_0 w_i^2 d_{33} E_p}{k_i}\left(a_{10}E_{s1}^*(x) + a_{1,-1}E_{s2}^*(x)\right)
\end{aligned} . \qquad (14)$$

Eq. (14) can be written in matrix form as

$$\frac{d^2}{dx^2}\begin{bmatrix} E_{s1}(x) \\ E_{s2}(x) \end{bmatrix} = \frac{4\mu_0^2 w_s^2 w_i^2 d_{33}^2 |E_p|^2}{k_s k_i}\begin{bmatrix} |a_{10}|^2 + |a_{11}|^2 & a_{11}a_{10}^* + a_{10}a_{1,-1}^* \\ a_{10}a_{11}^* + a_{1,-1}a_{10}^* & |a_{10}|^2 + |a_{1,-1}|^2 \end{bmatrix}\begin{bmatrix} E_{s1}(x) \\ E_{s2}(x) \end{bmatrix}. \qquad (15)$$

For a given $d_{33}(\boldsymbol{r})$, if we can choose the origin of the unit cell such that a_{10}, a_{11}, and $a_{1,-1}$ are all real and positive, and let $a_{11} = a_{1,-1}$, the square roots of the eigenvalues of the matrix are a_{10} +

#94772 - $15.00 USD Received 7 Apr 2008; revised 2 Jun 2008; accepted 12 Jun 2008; published 17 Jun 2008

a_{11} and $|a_{10} - a_{11}|$. The effective nonlinear coefficient is the square root of the larger eigenvalue of the matrix. Therefore,

$$d_{eff} = (a_{10} + a_{11})d_{33} . \quad (16)$$

Note that this is different from $\sqrt{a_{10}^2 + a_{11}^2 + a_{1,-1}^2}$, the gain due to common signal contribution from $\boldsymbol{G_{10}}$, $\boldsymbol{G_{11}}$, and $\boldsymbol{G_{1,-1}}$ as derived in Eq. (11). This is because the mechanism is different from a straight-forward common-signal interaction.

In general $2a_{10} > a_{11}$ so that the signal gain at this point is larger than purely from common signal interaction. Note that generally the parametric gain in a 2D NPC is smaller than in the 1D case [3,7]. However, because of these enhancements to the gain we show below with a specific example that in certain configurations the gain can reach that of the 1D QPM case.

4. Numerical simulation

We illustrate the effects and consequences of the overlapping gain by way of a 2D PPLN crystal that has a hexagonal inverted domain pattern with a filling ratio of 18.75% [10] as shown in Fig. 4. The dimensions of the unit cell are 29.5 x 29.5 μm^2. Also shown in Fig. 4 is the pattern of the perfect case of a square inverted domain (a filling ratio of 25%). The normalized Fourier coefficients a_{mn} in Eq. (6) for these two patterns can be calculated and the values for m=1, n=0, ±1 are shown in Table 1. For reference, the coordinates (λ_s, θ_s) for the points of intersection A-F in Fig. 2 for this pattern are given in table 2. We now proceed to calculate the optical parametric gain and the corresponding output wavelength for a singly-resonant OPO that resonates at the signal wavelength.

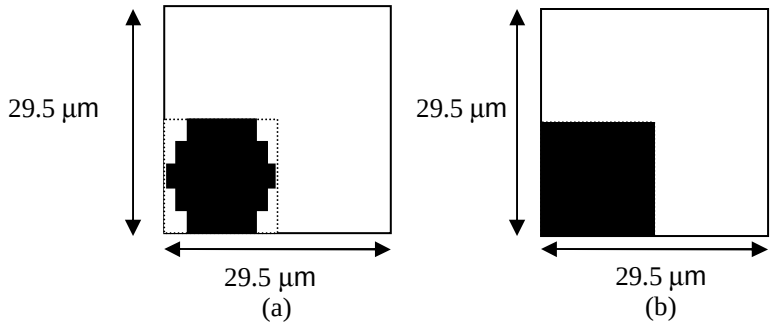

Fig. 4. (a) Hexagonal inverted domain in the simulation. (b) Square inverted domain. The small dashed square is half the size of the period.

Table 1. The Fourier coefficients a_{mn} of the first 3 terms of equation 6 for Fig. 4 (a) and (b)

	a_{10}	a_{11}	$a_{1,-1}$
(a)	0.2876	0.1902	0.1902
(b)	0.3183	0.2026	0.2026

#94772 - $15.00 USD Received 7 Apr 2008; revised 2 Jun 2008; accepted 12 Jun 2008; published 17 Jun 2008

Table 2. The signal wavelength and QPM direction relative to $\boldsymbol{G}_{10}$ for the points A-F in Fig. 2 for the 2D PPLN crystal used in the numerical example.

	A	B	C	D	E	F
Signal angle (°)	0	0.970	0	1.438	0.714	0.714
Signal wavelength (μm)	1.5484	1.5745	1.6416	1.5891	1.5788	1.5788

In a 2D NPC OPO, satisfying the QPM condition means that the pump, signal and idler are non-collinear with the exception of the case of QPM with the reciprocal vector $\boldsymbol{G}_{10}$. A finite pump beam size will hence lead to walk-off in the spatial overlap of the pump, signal and idler beams. In view of this the analytic form shown in Eq. (9) is not adequate in describing the parametric gain. In this simulation we take into account the beam walk-off to mimic the case of a real experiment. Because the periodic domain varies in the x-y plane and propagation of the beams lie only in that plane, the change caused by the parametric interaction to the z-dependence of the field is negligible and can be ignored in the present consideration. For every x, the fields are a function of y. We fix the pump beam to propagate in the x direction, parallel to $\boldsymbol{G}_{10}$ of the QPM pattern. The pump beam is assumed to be Gaussian. We include a flat-flat linear optical cavity whose axis in free space is at an angle θ_m relative to $\boldsymbol{G}_{10}$. The mirror angle θ_m determines the direction of the signal beam that travels at an angle relative to the pump beam inside the crystal. Since the signal direction in free space is normal to the cavity mirror, for small angles this angle in the 2D NPC will be equal to θ_m divided by the refractive index of the material. Therefore, we define a signal angle $\overline{\theta_s} \equiv \theta_m / n$ which for infinitely narrow beams is equal to θ_s. With this cavity we calculate the roundtrip signal gain of each signal wavelength. This in essence will be the single-pass parametric amplification gain for a given $\overline{\theta_s}$ and a finite pump beam diameter.

We use broadband white noise as the initial input signal and idler. The pump, signal and idler fields interact in the crystal as described by Eq. (5). The waves exit the crystal and the signal is reflected by the cavity mirrors and re-enters the crystal. The mirrors and the crystal are assumed broadband and lossless. The increase in the signal intensity is calculated following each pass through the crystal to obtain the roundtrip parametric gain. In the beginning the signal build-up is small as a large portion of the "noise" signal is not phase-matched and is dissipated. After several round trips, the increase in signal intensity and therefore the gain reaches a stable value. Eventually the gain decreases due to the depletion of the pump beam. The stable value before pump depletion is then the parametric gain for the selected $\overline{\theta_s}$ direction in this 2D NPC. The calculation is repeated over a range of wavelengths to map out the gain as a function of signal wavelength at a given $\overline{\theta_s}$ and this leads to a gain spectrum. The wavelength with the highest gain in the spectrum is the output signal wavelength for a free-running OPO at the given $\overline{\theta_s}$.

The result of the calculation is shown in Fig. 5 which displays the gain coefficient expressed as the gain-length product gL in color-coded amplitude as a function of the signal wavelength and the angle $\overline{\theta_s}$. This gain is calculated for a Gaussian pump beam waist w_0 of 160 μm ($E_p(y) = E_p(0)\exp(-y^2/w_0^2)$). The crystal length is 2.69 cm. The cavity length is 5.5 cm and the peak intensity is 90 MW/cm^2. These quantities are chosen to match crystals that can readily be fabricated. To help with interpreting the result, we superimpose on the figure the tuning curve (solid lines) from Fig. 2. It is immediately obvious that there are three curves for the gain with close but not exact overlap with the tuning curves corresponding to QPM by $\boldsymbol{G}_{10}$, $\boldsymbol{G}_{11}$, and $\boldsymbol{G}_{1,-1}$. To help with the analysis of this figure, we plot the largest gL product for each angle θ_s in Fig. 6(a) and the wavelength that corresponds to the largest gain at the corresponding angle in Fig. 6(b). Also shown is the curve for the second largest gain peak for

#94772 - $15.00 USD Received 7 Apr 2008; revised 2 Jun 2008; accepted 12 Jun 2008; published 17 Jun 2008

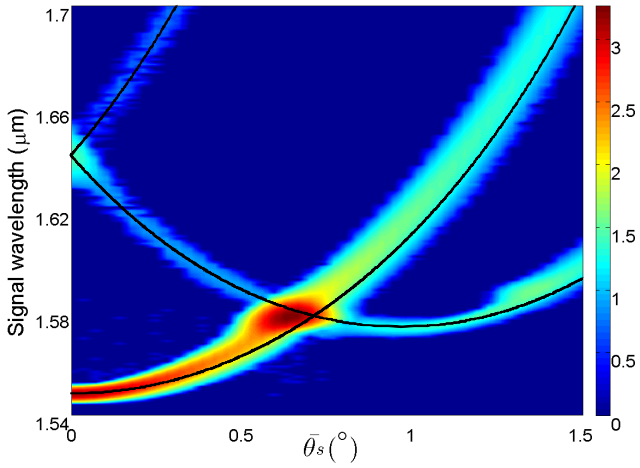

Fig. 5. The gain-length product gL as a function of signal wavelength and $\bar{\theta}_s$. w_0 = 160 μm. The solid lines are the QPM solution of $\boldsymbol{G_{10}}$, $\boldsymbol{G_{11}}$, and $\boldsymbol{G_{1,-1}}$.

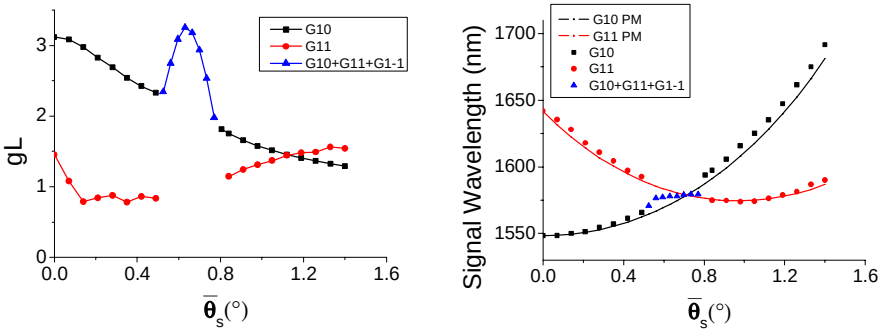

(a) (b)

Fig. 6. The gain-length product gL (a) and the output signal wavelength (b) versus $\bar{\theta}_s$. w_0 = 160 μm. The solid lines in the right figure are the QPM solutions for $\boldsymbol{G_{10}}$ and $\boldsymbol{G_{11}}$, respectively from the Sellmeier equations of PPLN.

the angle. We see now that gL for $\boldsymbol{G_{10}}$ is largest at $\bar{\theta}_s = 0°$. As $\bar{\theta}_s$ increases, the gain falls off because of increasing walk-off between the pump and the signal. The curve with a lower gain corresponds to QPM by $\boldsymbol{G_{11}}$. At $\bar{\theta}_s = 0°$ this gain benefits from a common-signal enhancement (point C in Fig. 2 and Eq. (11)) and results in a peak there. But this gain is less than that for $\boldsymbol{G_{10}}$ because the d_{eff} is smaller and the idler is off-angle and walks off to result in a smaller gain for the signal. Away from $\bar{\theta}_s = 0°$ the gain due to $\boldsymbol{G_{11}}$ is naturally smaller than for $\boldsymbol{G_{10}}$ since the Fourier coefficient for higher order QPM is smaller.

The most unique and significant part of this 2D NPC gain is in the region between $\bar{\theta}_s = 0.5°$ and 0.8° in the vicinity that corresponds to point E in the tuning curve. We can see from both Fig. 5 and Fig. 6(a) that the two gain curves merge into one and the gain shows a prominent peak at $\bar{\theta}_s$ close to that for point E. As explained in the previous section this is a consequence of the simultaneous coupled interaction of $\boldsymbol{G_{10}}$, $\boldsymbol{G_{11}}$, and $\boldsymbol{G_{1,-1}}$ that dominates the gain in this region. The enhancement here is substantial and results in a large increase of the calculated gL in this region to a value that is higher than that of $\boldsymbol{G_{10}}$ at 0°. As $\bar{\theta}_s$ exceeds 0.8°, the gain of $\boldsymbol{G_{10}}$ continues to fall off, while the gain of $\boldsymbol{G_{11}}$ slightly increases because of

#94772 - $15.00 USD Received 7 Apr 2008; revised 2 Jun 2008; accepted 12 Jun 2008; published 17 Jun 2008

reduced walk-off between signal and idler (point B). There is a small peak close to 1.4° that is a result of common-idler enhancement (point D and Eq. (13)).

Examination of the peak gain and the output wavelength at each $\bar{\theta}_s$ in the figures shows several interesting and unanticipated phenomena. Firstly, the entire gain curve exhibits a clear deviation from the tuning curve calculated from the Sellmeier equations. Analysis of the signal build-up in the cavity shows that this is a consequence of the dynamic build-up process of the signal in a beam with a finite size in the presence of beam walk-off. The transverse intensity of the signal beam is pulled toward the direction of the idler as the signal grows inside the crystal because of the walk-off. In order to make the signal beam return to the same point after a round trip, the cavity compensates this pull by choosing a direction for the signal that is slightly away from the idler direction that would have been determined by the tuninig curve. As a result of this balancing act, the signal wavelength is shifted to a value higher than that given by the tuning curve. Note that the degree of the pull increases with the beam diameter and the amount of this shift will increase with the size of the pump beam. Secondly the location of the highest gain in the region between $\bar{\theta}_s = 0.5°$ and $0.8°$ is shifted away from

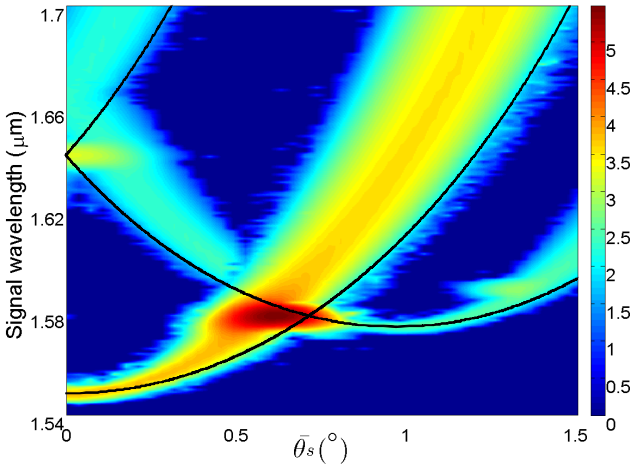

Fig. 7. The gain-length product gL as a function of signal wavelength and signal angle. w_0 = 1000 μm. The solid lines are the QPM solution of $\boldsymbol{G_{10}}$, $\boldsymbol{G_{11}}$, and $\boldsymbol{G_{1,-1}}$.

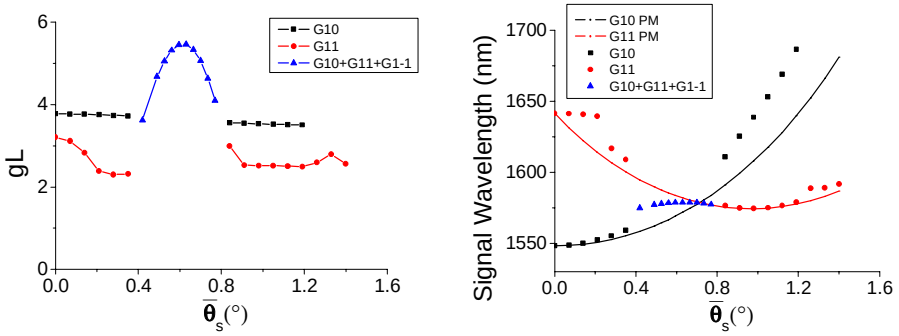

(a) (b)

Fig. 8. The gain-length product gL (a) and the output signal wavelength (b) versus $\bar{\theta}_s$. w_0 = 1000 μm. The solid lines in the right figure are the QPM solutions for $\boldsymbol{G_{10}}$ and $\boldsymbol{G_{11}}$, respectively from the Sellmeier equations of PPLN.

#94772 - $15.00 USD Received 7 Apr 2008; revised 2 Jun 2008; accepted 12 Jun 2008; published 17 Jun 2008

the point of intersection of the two tuning curves at 0.714° to 0.67°. Since $\boldsymbol{G_{10}}$ is a major contributor to this gain, the shift of the peak location can be explained by a rapid tailing off of the gain due to $\boldsymbol{G_{10}}$ as $\overline{\theta_s}$ increases. Finally, in that same region the signal wavelength makes a jump from a smooth progression to a value close to that associated with the highest gain, one that is provided by the triple interaction against that from $\boldsymbol{G_{10}}$ or $\boldsymbol{G_{11}}$ alone. This is a case of frequency pulling in the presence of multiple coupled interactions in an optical cavity that is commonly seen in laser cavities [11]. Yet the magnitude of the shift of more than 10 nm as shown here is probably unprecedented.

In order to distinguish the source of the shifts in Fig. 5 described above between walk-off of the signal beam and the pump beam that is inherent in QPM of 2D NPCs from that due to a finite pump beam size, we calculated the gain and wavelengths for the case of w_0 = 1000 μm. The results are shown in Fig. 7 and Fig. 8. At 1000 μm, the beams remain overlapped substantially over the course of the length of the crystal. Effects limited by the beam size are nearly eliminated. This results in a rather flat *gL* curve for each $\boldsymbol{G}$ vector. At 0° , 0.7° , and 1.4° , the phenomena of enhanced gain and shifts in signal wavelength when multiple reciprocal vectors act together are prominently displayed: The gains rise up at these angles and there is a stronger pull on the signal wavelength toward those where the gain peaks. In Table 3 we compare the normalized d_{eff} derived from the calculated *gL* product for various w_0 at points A~E for the inverted domains pattern of Fig. 4(a). Clearly $\overline{d_{eff}}$ approaches the value derived with plane-wave approximation as w_0 increases. Significantly d_{eff} at point E is consistently larger than that of $\boldsymbol{G_{10}}$. Its value is only 22% less than that of the relative 1D QPM value of 0.61 when the pump beam size is large and this is even with a realistic filling ratio of 18.75%. A perfect square domain would give a d_{eff} that nearly matches the 1D value. And the increased deviation from the calculated tuning curve confirms the physical picture of deviation given in the above paragraph.

Finally, it should be obvious that due to symmetry of the inverted domain pattern, the curves in Fig. 5 to Fig. 8 mirror themselves for negative values of $\overline{\theta_s}$.

Table 3. The normalized effective nonlinear coefficient $\overline{d_{eff}} = d_{eff} / d_{33}$ for various beam radiuses.

Beam waist (μm) / Point	160	320	500	1000	Infinity (plane-wave approximation)
A	0.2301	0.2593	0.2696	0.2789	0.2876
B	0.0959	0.1479	0.1688	0.1844	0.1902
C	0.1042	0.1643	0.1948	0.2306	0.2690
D	0.1666	0.2109	0.2329	0.2538	0.2690
E	0.2885	0.3823	0.4178	0.4496	0.4778

5. Conclusion

We have analyzed optical parametric interaction in a 2D NPC. While in general the nonlinear coefficient is small compared to a 1D NPC, we showed that at numerous orientations and wavelengths a multitude of reciprocal vectors contribute additively to enhance the gain in optical parametric amplification and oscillation in a 2D patterned crystal. In particular, we have derived the effective nonlinear coefficients for common-signal amplification and common-idler amplification for a tetragonal inverted domain pattern. We showed that in the specific case of a common-signal amplification with QPM by both $\boldsymbol{G_{10}}$ and $\boldsymbol{G_{11}}$, symmetry of the crystal results in coupled interaction with the corresponding common-signal amplification

#94772 - $15.00 USD Received 7 Apr 2008; revised 2 Jun 2008; accepted 12 Jun 2008; published 17 Jun 2008

by $\boldsymbol{G_{10}}$ and $\boldsymbol{G_{1,-1}}$. As a consequence, this coupled utilization of all three reciprocal vectors leads to an effective nonlinear coefficient that is larger than that of additive common-signal amplification using $\boldsymbol{G_{10}}$, $\boldsymbol{G_{11}}$, and $\boldsymbol{G_{1,-1}}$. We demonstrated with a numerical example using a PPLN crystal that a gain that comes close to that of a 1D QPM crystal could be realized in a 2D NPC with an inverted tetragonal domain pattern.

This special mechanism produces two pairs of identical signal and idler beams propagating in mirror-imaged forward directions. This is not possible with traditional 1D parametric devices. In conjunction with the gain enhancement and multiple beams output we also predict that there is a large pulling effect on the output wavelength and direction due to dynamic signal build-up in a noncollinear geometry that is intrinsic to the 2D NPC OPO.

We should point out that the output wavelength in this special 2D NPC is tunable just as with other NPC OPOs by changing the temperature or the grating period of the crystal. The parameters we have chosen in the simulation were based on realistic conditions so that the results of our analysis can be readily verified by a laboratory experiment.

In addition to emitting naturally separated pump, signal, and idler beams the high gain coupled with simultaneous emission of a dual pair of signal (and idler) beams of identical wavelengths in the 2D NPC OPG/OPO might find interesting applications in quantum information processing, providing a dual pair of entangled photons.

We thank Chien-Jen Lai for helpful discussions. This work was supported by the Nanoscience and Technology Program managed by the National Science Council under grant no. NSC 95-2120-M-001-006.

#94772 - $15.00 USD Received 7 Apr 2008; revised 2 Jun 2008; accepted 12 Jun 2008; published 17 Jun 2008